3rd Specialty Conference on Material Engineering & Applied Mechanics
3e Conférence spécialisée sur le génie des matériaux et mécanique appliquée

Montréal, Québec
May 29 to June 1, 2013 / *29 mai au 1 juin 2013*

Hysteretic Inelastic Behavior of Thin Steel Plates

Iraj H.P. Mamaghani
Ph.D, P.Eng., Associate Professor
Department of Civil Engineering, University of North Dakota
243 Centennial Dr., Grand Forks, ND, 58202-8115, USA
Iraj.mamaghani@engr.und.edu

Abstract: This paper deals with the inelastic analysis and behavior of thin steel plates subjected to in-plane cyclic compression and tension using the finite element method. The modified two-surface plasticity model and the approximate updated Lagrangian description of motion are employed, respectively, for material and geometrical nonlinearities in the inelastic finite element formulation for plates. The plate element is implemented in the computer program FEAP used in the analysis. The formulation accounts for the important cyclic characteristics of structural steel within the yield plateau and hardening regime, such as the decrease and disappearance of the yield plateau, reduction of the elastic range, and cyclic strain hardening, as well as the spread of plasticity through the thickness and plane of the plate. The cyclic performance of the formulation was found to be good when compared with the results obtained from the EPP, KH, and IH material models. Based on the results of an extensive parametric study, the effects of residual stresses, initial imperfection, width-thickness ratio, and loading history on the hysteretic behavior of thin steel plates are discussed and evaluated.

1 Introduction

Thin-walled steel structures are vulnerable to damage caused by the coupled instability, i.e., the interaction of local and overall buckling, in the event of a major earthquake. For example, Fig. 1 shows a steel bridge pier of hollow box section, which suffered severe local buckling damage near the base of the pier in the Kobe earthquake. When structural members are composed of thin-walled steel plate elements, the local buckling of the component plates may influence the strength and ductility of those members (Mamaghani, 2012). To this end, in designing thin-walled steel structures, it is very important to clarify the cyclic inelastic behavior of the component plates.

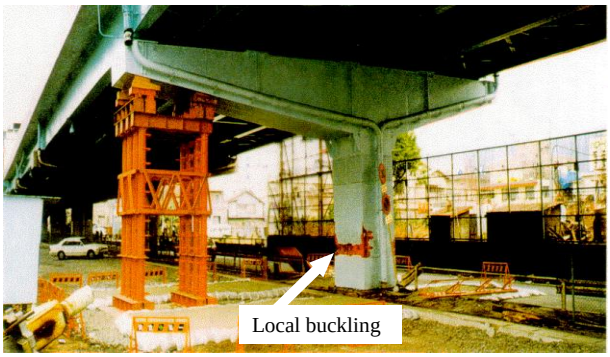

Figure 1: Local buckling of steel bridge pier, Kobe Earthquake, January 1995.

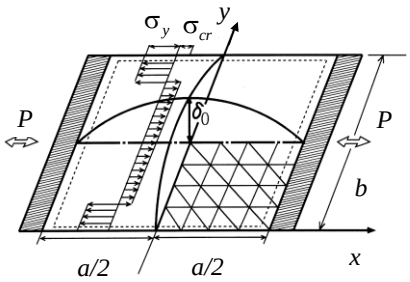

Figure 2: Simply supported rectangular plate modeling flange of the pier.

On the other hand, the stress-strain relationship used in cyclic structural analyses depends on the loading history to which the structure or structural members are subjected. Therefore, advanced computational methods, such as the finite element method (FEM), require an accurate and refined constitutive law to account for the general cyclic behavior of structural steel, which has a characteristic yield plateau followed by strain hardening. The main objective of this study is to use the modified two-surface plasticity model (2SM), recently developed by the author and his coworkers (Mamaghani et al. 1995, Shen et al. 1995), for material nonlinearity to trace the cyclic inelastic behavior of simply supported rectangular thin steel plates using the FEM. An elastoplastic finite element formulation for plates, considering geometrical and material nonlinearities, is developed and implemented in the computer program FEAP (Zienkiewicz 1977) used in the analysis. The 2SM is employed for material nonlinearity. The approximate updated Lagrangian description of motion (AULD) (Washizu 1982) is adopted for geometrical nonlinearity. The formulation accounts for the important cyclic characteristics of structural steel within the yield plateau and strain hardening regime, such as the decrease and disappearance of the yield plateau, reduction of the elastic range, and cyclic strain hardening, as well as the spread of plasticity through the thickness and plane of the plate.

The main parameters concerned in the analysis are: residual stress; initial deflection; width-thickness ratio; and loading history. In what follows, the numerical method used in the analysis is first briefly explained. Later, the cyclic elastoplastic performance of the formulation is discussed and compared with results obtained from the elastic-perfectly plastic (EPP), the kinematic hardening (KH), and the isotropic hardening (IH) material models. Based on the results of analysis, the effect of each material model and aforementioned parameters on the hysteretic behavior (buckling/plastic collapse and energy absorption capacity) of thin plates is discussed and evaluated.

2 Numerical Method

Assuming plane-stress state, the discrete Kirchhoff triangular (DKT) element for plate bending combined with the constant strain triangle (CST) element for plate membrane is employed in this study (Bathe and Ho 1981; Fafard et al. 1989). The material nonlinearity is defined by the 2SM. The AULD, in which the configuration of the structure at the beginning of each incremental loading step is approximated by a flat plate element (Jetteur et al. 1983), is employed for the geometrical nonlinearity. The three points Gauss quadrature integration formula is used to integrate the element stiffness equations for the plate element. A layered approach is employed to consider the plastification of thickness at integration points by assuming seven layers across the plate thickness (Bathe and Ho 1981).

According to the algorithm discussed above, an elastoplastic plate element subroutine was coded and implemented in the computer program FEAP used in the analysis. The Newton-Raphson iterative scheme

coupled with the incremental displacement control is employed in the analysis (Zienkiewicz 1977; Owen and Hinton 1980). The incremental uniform displacement is applied on the plate's edge. The displacement convergence criterion is adopted in the analysis and the convergence tolerance is taken as 10^{-3} (Zienkiewicz 1977). The details of the process for numerical analysis can be found in a work by Mamaghani (1996). In what follows, the analyzed plate members and numerical results will be presented and discussed.

2.1. Analytical Modeling

Throughout the numerical study, the assumed analytical model for plates is considered as shown in Fig. 2. The plate has an aspect ratio of *a/b* = 0.7, and is taken to be simply supported along the four edges. *a* and *b* are the length and width of the plate. All edges are assumed to remain straight when subjected to in-plane displacement; that is, at $x = -(a/2)$ and $(a/2)$, $w = \theta_x = \theta_z = 0$; and at y = 0 and *b*, $w = \theta_y = 0$. Such a plate is thought to be modeling component plates in steel hollow box section members (see Fig. 1). The width-thickness ratios of *b/t* = 20, 40, 60, 80 are assumed in the analysis. The initial out-of-flatness of

$$[1] \qquad \delta = \delta_0 \cos(\frac{\pi x}{a}).\sin(\frac{\pi y}{b})$$

in which $\delta_0 = b/450$, is assumed in the analysis (see Fig. 2). The assumed value of δ_0 is considered to be an average value in practical unstiffened plates (Usami 1993). The material chosen is structural steel of grade JIS SS400 (equivalent to ASTM A36) with the properties of the Young's modulus *E* = 207 GPa, yield stress $\sigma_y = 274$ MPa, Poisson's ratio $\upsilon = 0.29$, length of yield plateau $\varepsilon_{st}^p = 12\varepsilon_y$ ($\varepsilon_y =$ yield strain of the material), and plastic modulus at the initial hardening $E_{st}^p = 0.025E$. The 2SM parameters for SS400 are given by Mamaghani (1996) and Shen et al. (1995).

The pattern of assumed residual stress distribution over the cross-section is shown in Fig. 2, and is uniform along the entire length of the plate. The tensile and compressive residual stresses are taken as $\sigma_{rt} = \sigma_y$ and $\sigma_{rc} = (1/3)\sigma_y$, respectively. From the symmetry conditions, a quarter of the plate is analyzed, dividing this part into 4×4 elements, as shown in Fig. 2. A forced displacement is imposed along loading edges incrementally, and the increments in reaction forces are calculated at every step. The average in-plane edge strain, $\bar{\varepsilon}$, and stress, $\bar{\sigma}$, over the cross section are defined as $\bar{\varepsilon} = (\Delta a/a)$ and $\bar{\sigma} = (P/bt)$, where $\Delta a =$ increment of displacement amplitude along *x*-axis; P = reaction force along the loading edge; and *t* = plate thickness. The incremental displacement amplitude of $\Delta a = 1.0\times10^{-4}(a/2) - 0.5\times10^{-5}(a/2)$ is adopted in the analysis.

2.2. Cyclic Loading

Constant displacement amplitude (CDA) loading is used in the analysis, as shown in Fig. 3a. The plate is first subjected to compressive shortening of $m\varepsilon_y$ at the loading edge. This is defined as 0.5 cycles (see Fig. 3b). Note that the compressive strain is assumed to be positive. Then, the plate is unloaded in the compression side and reloaded in the tension side until it is stretched up to $-m\varepsilon_y$. This stage of loading is defined as 1.0 cycle. Similarly, the other cycles, 1.5, 2.0, 2.5 and so on, are defined as shown in Fig. 3b. The normalized maximum average strain, *m*, at the loading edge of the plate is defined as

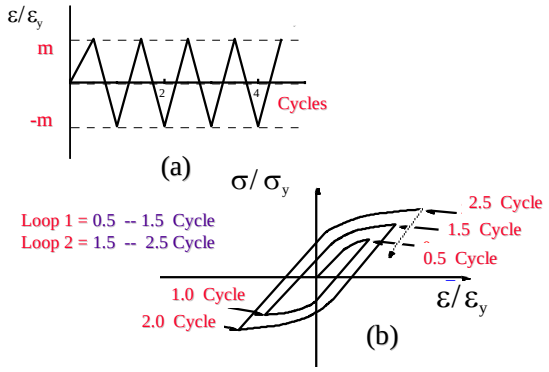

Figure 3: Loading program and definition of cycles and loops.

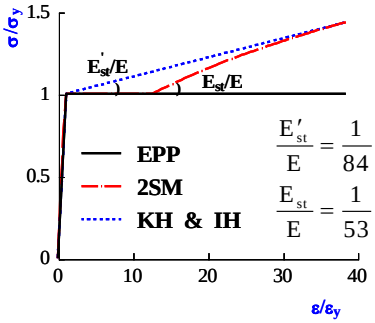

Figure 4: Bilinear stress-strain relationship for steel using different material models.

[2] $$m = \frac{\bar{\varepsilon}_{max}}{\varepsilon_y}$$

in which $\bar{\varepsilon}_{max}$ = maximum average strain. Three patterns of loading with m = 2, 4, and 6 are adopted for CDA loading, and cycling was performed up to 4.5 cycles.

2.3. Material Models

Figure 4 shows the uniaxial stress-strain relationship under monotonic loading for SS400 steel using the 2SM, EPP, KH, and IH material models. In the present study, based on the experimental results for SS400 steel (Mamaghani et al. 1995), the kinematic and isotropic hardening rates are assumed as E'_{st}/E=1/84, which is considered equal to the slope of the line joining the initial yield point to the loading point corresponding to 5% axial strain obtained by using the 2SM (see Fig. 4).

3 Numerical Results

A series of elastoplastic large deflection analyses are performed on hypothetical specimens of simply supported rectangular plates by imposing in-plane strain cycles of constant displacement amplitudes using the analysis scheme described above. In what follows, numerical results will be presented and discussed.

3.1. Effect of Residual Stress

As a typical example, Fig. 5 shows the hysteretic curves obtained using the 2SM for the two specimens with and without residual stresses. For both specimens the b/t ratio is 40 and m = 4. The normalized average in-plane stress, $\bar{\sigma}/\sigma_y$, is taken as the ordinate, and the corresponding normalized average edge strain, $\bar{\varepsilon}/\varepsilon_y$, is taken as the abscissa (see Fig. 5a). Note that, in what follows, the $\bar{\varepsilon}/\varepsilon_y$ is assumed positive when the plate is subjected to compressive shortening on the loaded edge. Fig. 5b compares the analytical averaged axial stress $\bar{\sigma}$-center deflection, w, relationship for both specimens. As the edge strain, $\bar{\varepsilon}/\varepsilon_y$, increases, the path of hysteretic curves enters the post buckling range through the elastic limit point, at which yield penetration begins in the most stressed element of the plate (see Fig. 5a). Whereas the edge strain increases, the average in-plane load decreases after the peak stress point (see Fig. 5a) of the plate is achieved. The results in Fig. 5a indicate that the initial buckling load decreases by 13% due to residual stresses. Fig. 5a shows that the initial yielding of the plate occurs earlier when the

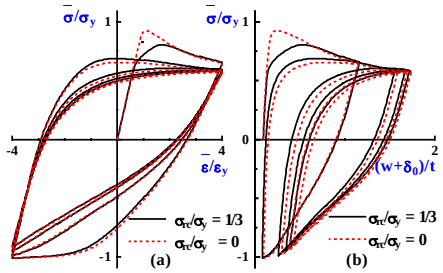

Figure 5: Effect of residual stress: (a) $\bar{\sigma}/\sigma_y - \bar{\varepsilon}/\varepsilon_y$; (b) $\bar{\sigma}/\sigma_y - (w+\delta_0)/t$.

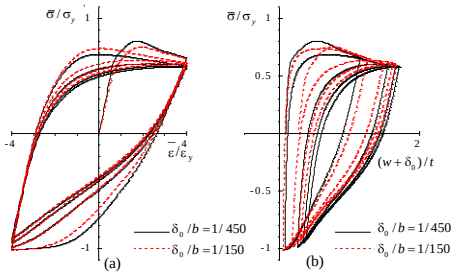

Figure 6: Effect of initial deflection: (a) $\bar{\sigma}/\sigma_y - \bar{\varepsilon}/\varepsilon_y$; (b) $\bar{\sigma}/\sigma_y - (w+\delta_0)/t$.

residual stress is considered in the analysis. This results in a lower stiffness of the stress-strain curve (see Fig. 5a). On the other hand, the stress-strain curve without residual stress shows a steeper descending slope due to buckling, and the curves in both cases (with and without residual stress) coincide at the point corresponding with $\bar{\varepsilon}/\varepsilon_y$=2.0, see Fig. 5a. The obtained results indicate that the residual stresses have almost no effect on the subsequent cyclic behavior (see Fig. 5a) and the progress of buckling (see Fig. 5b) of the plate.

3.2. Effect of Initial Deflection

Figure 6 shows the effect in change of the initial deflection on the cyclic behavior of plates for the two specimens with $\delta_0/b = 1/450$ and $\delta_0/b = 1/150$, respectively. The result in this figure shows that an increase in the initial deflection mainly has the effect of decreasing the initial buckling load and does not significantly affect the subsequent cyclic behavior. It is worth noting that the numerical studies on the cyclic inelastic behavior of steel compression members by Mamaghani et al. (1996a, 1996b) and Banno et al. (1998) show the same behavior as discussed above and indicate that annealing and initial imperfection do not significantly affect overall behavior due to cycling.

3.3. Comparison between Two-Surface Model and Other Models

In this section, cyclic behavior of simply supported steel plates is analyzed using the 2SM and bilinear EPP, KH, and IH models. The aim is to compare the effect of each material model on the buckling/plastic collapse behavior of the plates. A typical loading program with CDA of *m* = 4.0 will be presented and discussed. For comparison, the selected plate parameters (*b/t* = 40, $\delta_0 = b/450$, and σ_{cr}/σ_y=1/3) are kept the same.

Figure 7 compares the analytical averaged axial stress $\bar{\sigma}$-averaged axial strain, $\bar{\varepsilon}$, and averaged axial stress $\bar{\sigma}$-center deflection, *w*, relationship for *m* = 4 obtained using the 2SM and bilinear EPP, KH, and IH material models duly normalized. As shown in Fig. 7a, the hysteretic loops have almost the same shape for all models except the 2SM. The loops for the EPP, KH, and IH models show a large elastic range for unloading in the tension side and reloading in compression side. Furthermore, the post-buckling parts of these curves have a steeper descending slope compared to that of the 2SM. Figure 8a compares the change in load-carrying capacity of the plate $\bar{\sigma}_{\max}$, during cyclic loading. In the case of the EPP, KH, and IH models, the calculated second and subsequent buckling load capacities are higher than those of the 2SM (see Figs. 7a and 8a). For the IH model, the maximum compressive load during cycling is higher than the other models and increases after 2.5 cycles because of the large cyclic strain hardening.

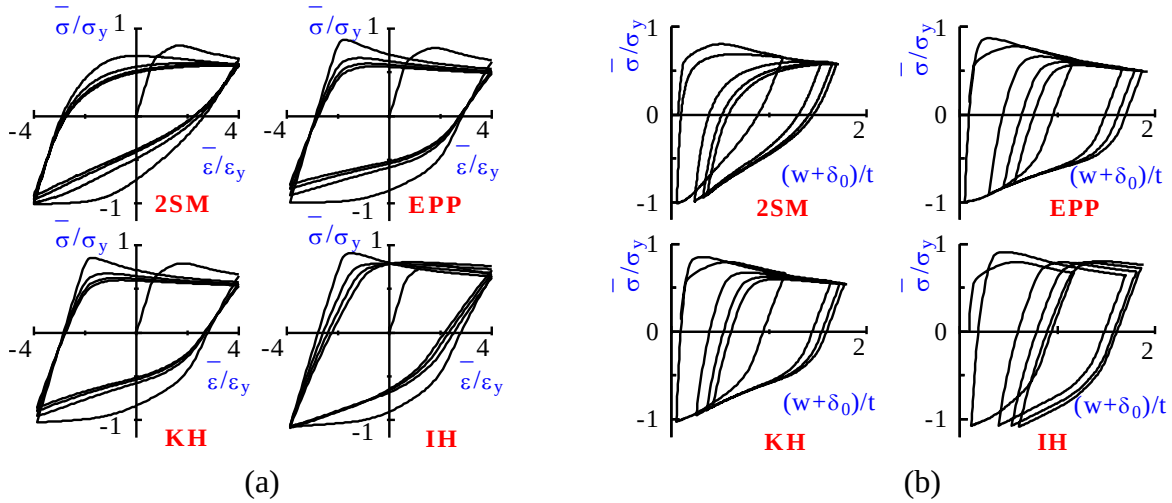

Figure 7: Comparison between 2SM and other models: (a) $\bar{\sigma}/\sigma_y - \bar{\varepsilon}/\varepsilon_y$; (b) $\bar{\sigma}/\sigma_y - (w+\delta_0)/t$.

Conversely, the rate of decrease in buckling loads slows down for the other models and tends to converge to $0.6\,\sigma_y$ (see Fig. 8a).

One significant feature of the hysteretic loops in Fig. 7a is that all of the models except the 2SM give the second buckling load higher than that of the initial one (see also Fig. 8a). The reason for this is that the EPP and IH models do not consider the Bauschinger effect due to plastic deformation, and the KH model takes the size of the elastic range to be constant, which does not represent the actual behavior of the structural steel (Mamaghani et al. 1997). In the case of the 2SM, the reduction of elastic range is taken accurately into account (Mamaghani et al. 1995, Shen et al. 1995), which has the effect of softening of the hysteresis curve (reduction in stiffness), leading to lower values of the buckling load. The cyclic compressive load capacities up to 2.5 cycles for the EPP and KH models are almost the same, as shown in Fig. 8a. This is because the strain hardening effect is canceled out by the Bauschinger effect in the KH model. However, the KH model exhibits a higher compressive load capacity due to cyclic strain hardening in subsequent cycles (see Fig. 8a).

Fig. 8b compares the progress of residual displacements $(\delta_{rd}+\delta_0)/t$, in the compression side $C \to T$ (buckling), and in the tension side $T \to C$, at plate center, versus the number of cycles, obtained from analyses using the 2SM, EPP, KH, and IH models for CDA (m = 4) loading history. From this comparison, it can be seen that the EPP, KH, and particularly the IH model grossly overestimate the residual displacements compared with the 2SM. As can be noticed from Figs. 7b and 8b, the progress of buckling, which affects significantly the maximum compressive load and subsequent cyclic behavior, is different for each material model. The results in Figs. 7a and 8a also indicate that the maximum yield strength in tension side decreases with an increase in the number of cycles for all models except the IH model. In the case of the IH model, in spite of the higher progress in buckling (see Figs. 7b and 8b), the maximum yield strength in the tension side does not decrease due to the large cyclic strain hardening. It is worth noting that behavior similar to that discussed previously, was observed for the axially loaded pin-ended bracing members with a solid rectangular section (Mamaghani et al. 1996a).

3.4. Energy Absorption Capacity

The normalized energy absorption capacity, defined here as E_i/E_e, is one of the objective measures of the overall inelastic behavior of a structural member under cyclic loading (Mamaghani et al. 1997). Therefore, in this section, it is used to describe and evaluate the performance of each material model in the

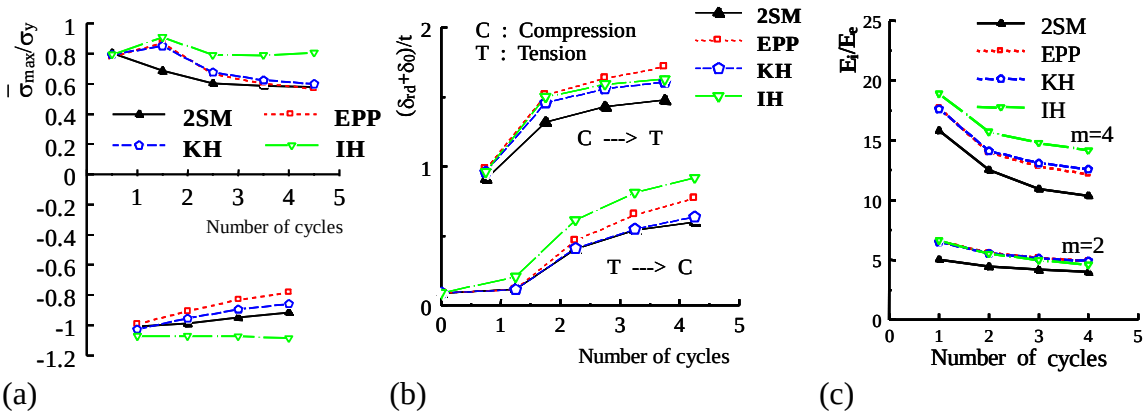

(a) (b) (c)

Figure 8: Comparison between 2SM and other models: (a) $\bar{\sigma}_{max}/\sigma_y$ - number of cycles; (b) $(\delta_{rd}+\delta_0)/t$ - number of cycles ; (c) E_i/E_e - number of cycles.

prediction of the hysteretic behavior for the analyzed plates. E_i is defined as the energy corresponding to the loop *i* (area enclosed by the $\bar{\sigma}-\bar{\varepsilon}$ curve). As shown in Fig. 3, the loop *i* = 1 starts at 0.5 cycles and ends at 1.5 cycles; the loop *i* = 2 is confined between 1.5 and 2.5 cycles, and so on. The elastic strain energy E_e is defined as $E_e = 0.5\sigma_y\varepsilon_y$. Using the above definitions, Fig. 8c compares the normalized energy absorption capacities, E_i/E_e, versus the number of loops, obtained from analyses using the 2SM, EPP, KH, and IH models for CDA (*m* = 2, 4) loading history. From this comparison, it can be seen that the EPP, KH, and particularly the IH model grossly overestimate the energy absorption capacity compared with the 2SM, especially as the number of cycles increases (see Fig. 8c). As shown in Fig. 8c, in the case of CDA with *m* = 2 (a relatively small displacement), the normalized energy absorption capacity for all models except the 2SM is almost identical; however, in the case of *m* = 4 (a large displacement), the normalized energy absorption capacity is much higher for the IH model due to the reasons discussed in the previous section. With the progress of deflection (see Figs. 7b and 8b), which has the effect of degrading buckling load (see Figs. 7a and 8a), the normalized energy absorption capacity in the fourth loop decreases by 20-30% compared with the first loop. The normalized energy absorption capacity reduces sharply in the second loop and tends to stabilize following the third loop under CDA (Fig. 8c).

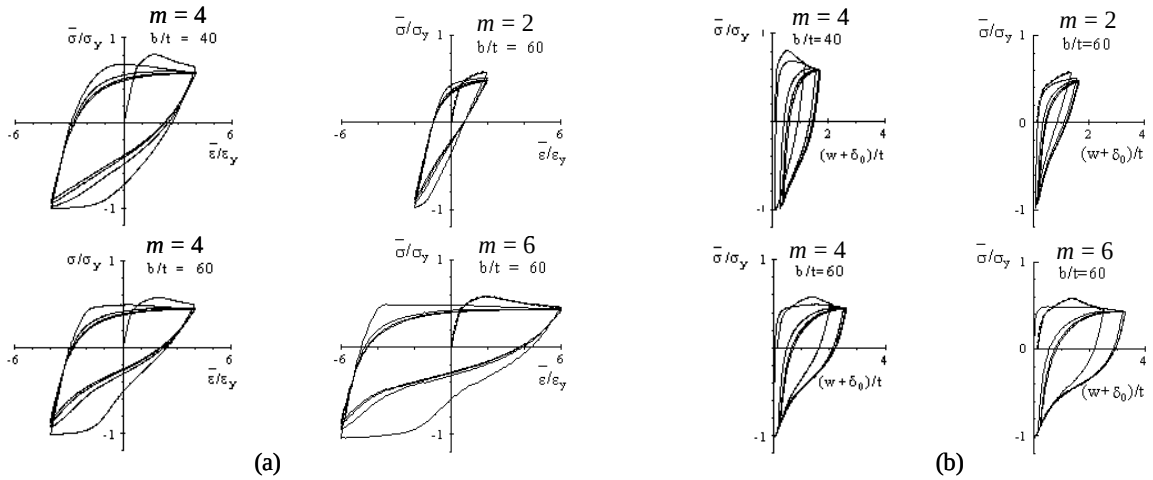

(a) (b)

Figure 9: Effect of width-thickness ratio and displacement amplitude: (a) $\bar{\sigma}/\sigma_y-\bar{\varepsilon}/\varepsilon_y$; (b) $\bar{\sigma}/\sigma_y-(w+\delta_0)/t$.

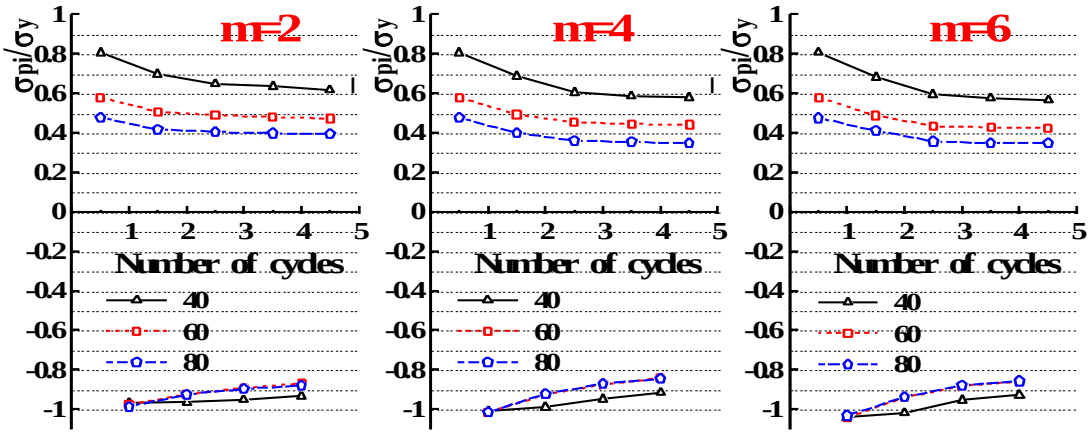

Figure 10: Effect of width-thickness ration (*b/t* = 40, 60, 80) and displacement amplitude (*m* =2, 4, 6) on load carrying capacity due to cycling under CDA (2SM).

Because the energy absorption capacity is of great interest in seismic design (it reduces the ductility demand on structure), it should be estimated as accurately as possible. From the above comparison between models, it is noticed that all models except the 2SM overestimate the energy absorption capacity. Therefore, the use of the EPP, KH, and IH models in the cyclic analysis of structures may lead to an erroneous estimate of energy absorption capacity. The 2SM, however, gives more promising results and can be used in the cyclic analysis of structures more confidently.

3.5 Effect of Width-Thickness Ratio and Displacement Amplitude

In this section, a series of numerical analyses on simply supported steel plates with three values of width-thickness ratios (*b/t* = 40, 60, 80) subjected to three loading programs of CDA (*m* = 2, 4, 6) are carried out to examine the effect of these parameters on the cyclic behavior. In the analysis, both the residual stresses and initial deflection of $\delta_0 / b = 1/450$ are considered. Fig. 9 shows the hysteretic curves obtained using the 2SM for the specimens of *b/t* = 40, 60 (*m* = 2, 4, 6). All plates have characteristics of a large thinning out of the hysteresis loops (unstable behavior) up to 2.5 cycles; however, the hysteresis loops tend to stabilize (stable behavior) in subsequent cycles, see Fig. 9a. The change in the normalized compressive load-carrying capacity $\bar{\sigma}_{pi}$ during cyclic loading is shown in Fig. 10. The results in this figure indicate that there is a large reduction in buckling load up to 2.5 cycles, but it converges to a certain value and does not significantly change in further cycles. The unstable behavior in the early cycles of loading is due to the large progress in buckling (i.e., the increase in deflection of the plate; see Fig. 9b) and the spread of plastic zone, which have the effect of reducing the plate stiffness. As shown in Fig. 9b, buckling of plates mainly occurs in the first compressive loading (0.5 cycles) and increases in the second compressive loading (1.5 cycles). There is no significant change in buckling after 2.5 cycles. Fig. 10 shows that with the increase in width-thickness ratio the cyclic load-carrying capacity decreases markedly. The reason for this, as shown in Fig. 9b, is that the size and rate of increase in buckling are larger for the plates with a large width-thickness ratio (thinner plates).

Figure 11 shows the effect of width-thickness ratio (*b/t* = 40, 60, 80) and displacement amplitude (*m* = 2, 4, 6) on the normalized energy absorption capacity of plates with the increase in the number of loading cycles under CDA. The absorbed energy for loop *i*, E_i, is normalized with the absorbed energy in the first loop E_1. The results in Fig. 11 indicate that: (1) the larger the width-thickness ratio, the smaller the normalized energy absorption capacity; (2) the reduction in the normalized energy in the second loop (1.5 to 2.5 cycles) is considerably large and tends to stabilize after the third loop for all *b/t* ratios and displacement amplitudes; (3) an increase in the displacement amplitude *m* causes a larger reduction in the normalized energy absorption capacity, especially in the second loop, due to the larger thinning out of

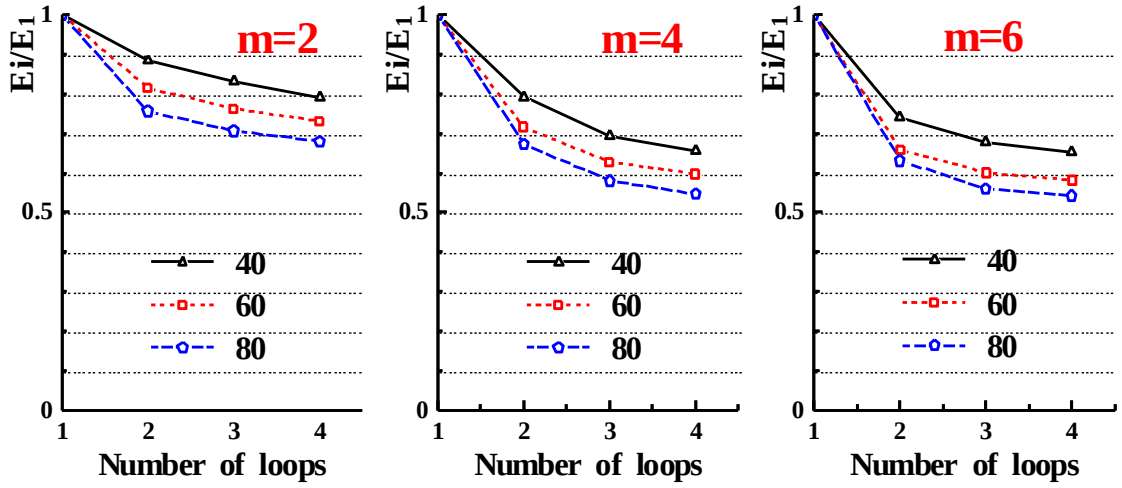

Figure 11: Effect of width-thickness ration (*b/t* = 40, 60, 80) and displacement amplitude (*m* =2, 4, 6) on energy absorption capacity due to cycling under CDA (2SM).

the hysteresis loops up to 2.5 cycles when the displacement amplitude is large; and (4) the rate of change in the normalized energy absorption capacity is not noticeably affected by the different values of *b/t* ratios following the second loop.

4 Conclusions

This paper deals with the cyclic inelastic behavior and large deflection analyses of simply supported thin steel plates using the finite element method. From the comparison between cyclic elastoplastic performances of different models discussed in this paper, it was concluded that the use of the EPP, KH, and IH models in the cyclic analysis of structures may lead to an erroneous estimate of cyclic behavior (maximum compressive load and energy absorption capacity). The 2SM, however, gives more promising results and can be used more confidently. From this study, it was also found that: (1) residual stress and increase in the initial deflection have mainly the effect of decreasing the initial maximum compressive load (buckling load) and does not significantly affect the subsequent cyclic behavior; (2) the EPP, the KH and particularly the IH models grossly over-estimate the energy absorption capacity compared to the 2SM; (3) the normalized energy absorption capacity reduces sharply in the second loop and tends to stabilize following the third loop under cyclic CDA loading; (4) the energy absorption and compressive load-carrying capacities markedly decrease under cyclic loading because of the increase in the width-thickness ratio. The reason for this is that the size and rate of increase in buckling and the spread of plastic zone are larger for plates with a large width-thickness ratio (thinner plates).

References

Banno, S., I. H.P. Mamaghani, T. Usami, E. Mizuno, 1998. Cyclic elastoplastic large deflection analysis of thin steel plates. *Journal of Engineering Mechanics, ASCE*, 124(4), 363-370.

Bathe, K. J., and L. W. Ho, 1981. A simple and effective element for analysis of general shell structures. *Computers and Structures,* Vol. 13, 673-681.

Bradford, M. A., and M. Azhari, 1995. Inelastic local buckling of plates and plate assemblies using bubble functions, *Engineering Structures*, 17(2), 95-103.

Fafard, M., G. Dhatt, , and J. L. Botaz, 1989. A new discrete Kirchhoff plate/shell element with updated procedures, *Computers and Structures*, Vol. 31(4), 591-603.

Jetteur, Ph., S. Cescotto, V. de Ville de Goyet, and F. Frey, 1983. Improved nonlinear finite elements for oriented bodies using an extension of Marguerre's theory, *Computers and Structures*, 17(1), 129-137.

Mamaghani, I. H. P., 1996. Cyclic elastoplastic behavior of steel structures: theory and experiment, *Ph.D. Thesis*, Nagoya University, Nagoya, Japan.
Mamaghani, I. H. P., C. Shen, E. Mizuno, and T. Usami, 1995. Cyclic behavior of structural steels. I: experiments, *J. Engrg. Mech.*, ASCE, 121(11), 1158-1164.
Mamaghani, I. H. P., T. Usami, and E. Mizuno, 1996a. Inelastic large deflection analysis of steel structural members under cyclic loading, *Engineering Structures*, UK, Elsevier Science, 18(9), 659-668.
Mamaghani, I. H. P., T. Usami, and E. Mizuno, 1996b. Cyclic elastoplastic large displacement behavior of steel compression members, *J. Structural Engineering*, JSCE, Vol. 42A, 135-145.
Mamaghani, I. H. P., T. Usami, and E. Mizuno, 1997. Hysteretic behavior of compact steel box beam-columns. Journal of Structural Engineering, JSCE, Japan, Vol. 43A, 187-194.
Mamaghani, I.H.P (2012), Cyclic Elastoplastic Large Displacement Analysis and Stability Evaluation of Steel Tubular Braces, *Journal of American Transaction on Engineering & Applied Sciences (ATEAS)*, pp. 75-90. http://tuengr.com/ATEAS/V01/75-90.pdf
Owen, D.R.J., and E. Hinton, 1980. *Finite Elements in Plasticity,* Pineridge Press Limited, Swansea, UK.
Shen, C., I. H. P. Mamaghani, , E. Mizuno, and T. Usami, 1995. Cyclic behavior of structural steels. II: theory, *J. Engrg. Mech., ASCE*, 121(11), 1165-1172.
Usami, T., 1993. Effective width of locally buckled plates in compression and bending, *J. Struct. Engrg., ASCE*, 119(5), 1358-1373.
Washizu, K., 1982. *Variational Methods in Elasticity and Plasticity,* 3rd Ed., Pergamon Press.
Zienkiewicz, O. C., 1977. *The Finite Element Method,* 3rd Ed., McGraw-Hill, New York.